First-principles search for *n*-type oxide, nitride, and sulfide thermoelectrics

Kevin F. Garrity[*]

Material Measurement Laboratory, National Institute of Standards and Technology, Gaithersburg, Maryland 20899, USA

Oxides have many potentially desirable characteristics for thermoelectric applications, including low cost and stability at high temperatures, but thus far there are few known high zT n-type oxide thermoelectrics. In this work, we use high-throughput first-principles calculations to screen transition metal oxides, nitrides, and sulfides for candidate materials with high power factors and low thermal conductivity. We find a variety of promising materials, and we investigate these materials in detail in order to understand the mechanisms that cause them to have high power factors. These materials all combine a high density of states near the Fermi level with dispersive bands, reducing the trade-off between the Seebeck coefficient and the electrical conductivity, but they do so for several different reasons. In addition, our calculations indicate that many of our candidate materials have low thermal conductivity.

I. INTRODUCTION

The need for clean efficient power generation has led to a renewed interest in thermoelectric materials, which can directly convert a temperature gradient into electrical power. Thermoelectrics can take advantage of a variety of heat sources, including solar or waste heat, to cleanly generate electricity [1–5]. Conversely, they could be used in cooling applications via the Peltier effect. There has been an extensive effort over recent years to discover and optimize materials with high zT, a dimensionless thermoelectric figure of merit. While there has been significant progress in this area, existing materials have not yet managed to provide a combination of high zT, low materials cost, and high durability that would result in widespread adoption. Much of the research on thermoelectrics has focused on high mobility semiconductors with small band gaps. Unfortunately, many of the most promising candidate materials have practical concerns (cost, toxicity, stability), which have thus far limited their use in applications [6].

In this work, we focus on the less explored group of wide band gap transition metal oxides, as well as related nitrides and sulfides. While oxides are not usually thought of as promising for thermoelectric applications, due to their typically low mobilities, the discovery of good thermoelectric performance in p-type Na_xCoO_2 and other layered Co-based materials resulted in an increased interest in this class of materials [1–3,7]. n-type materials such as ZnO and $SrTiO_3$ have also displayed high power factors, but their zT values have thus far been only moderate, due to high thermal conductivities [8–10]. Despite limited success thus far, oxides provide many potential advantages as thermoelectrics: (1) high thermal and chemical stability in air, (2) chemical versatility, allowing for extensive substitutions and doping, (3) low thermal conductivity, and (4) low cost materials and processing [1–3,6,11]. Thus far, much of the experimental work on oxide thermoelectrics has focused on a relatively small number of oxides, mostly binaries and perovskites, leaving open the possibility that better oxide thermoelectrics exist.

In this work, we use high-throughput density functional theory (DFT) calculations [12–22] to identify promising n-type thermoelectric oxides and related materials from the Inorganic Crystal Structure Database (ICSD) [23]. The large amount of work required to synthesize, optimize, and measure thermoelectrics experimentally make this type of theoretical screening of candidate materials particularly desirable. Similar techniques have been used successfully to study the thermoelectric behavior of a variety of materials, including oxides [24–35]. While a fully first-principles theoretical calculation of zT remains challenging, especially for oxides, which often have partially localized carriers, we can nevertheless screen materials for both electronic and vibrational properties that are necessary for good thermoelectric performance. In this work, we perform such a screening procedure, identifying many candidate materials with calculated thermoelectric properties that are similar to or surpass experimentally studied n-type oxides. Furthermore, we analyze the mechanisms behind the high thermoelectric performance of these materials, finding that they fall into a small number of groups with similar properties.

II. METHODS

A. Calculating thermoelectric performance

The dimensionless figure of merit for thermoelectrics can be written as

$$zT = \sigma S^2 T/\kappa, \tag{1}$$

where σ is the electrical conductivity, S is the Seebeck coefficient, κ is the total thermal conductivity (electrical plus lattice), and T is the temperature. The power factor, which determines the electrical response of a material to a temperature gradient, is $S^2\sigma$.

Unfortunately, the components of zT are not all easy to calculate using first-principles techniques. Within the constant relaxation time approximation, which is used in this work, S can be calculated from a band structure calculation without any adjustable parameters [36]. Within the same approximation, it is possible to calculate σ/τ_e, where τ_e is the electronic relaxation time. Unfortunately, calculating τ_e from first-principles remains challenging [37,38]. This problem is

---

*kevin.garrity@nist.gov

especially severe for oxides, which often display complicated conduction mechanisms and polaronic effects at low doping and low temperatures. In this work, we are concerned primarily with the opposite regime of high temperatures and high doping, where the carrier mobilities of oxides are typically larger [1–3]. Because we are comparing materials which are chemically similar, we expect them to have broadly similar electron scattering mechanisms. Therefore we will use the quantity $S^2\sigma/\tau_e$ to rank our candidate materials for suitability as thermoelectrics. This estimate, which has been used in many previous works [25,33,39], should be sufficient to at least screen materials for those with band structures that are promising for thermoelectric applications, even if determining the final ranking of materials will require experimental input.

For reference, first-principles techniques can reproduce the thermoelectric properties of SrTiO$_3$ with $\tau_e \approx 4$ fs at room temperature [32], a typical value for oxides, but some high mobility oxides like ZnO have much longer scattering times [40]. All wide band materials have to be doped in order to be used as thermoelectrics. In this work, we use the rigid band filling model to estimate the effects of doping, and we rank materials by $S^2\sigma/\tau_e$ at their optimum doping.

After identifying materials with promising band structures, we perform more computationally expensive phonon calculations for a limited number of candidate materials to estimate the lattice thermal conductivity, which is the dominant contribution to the thermal conductivity for most thermoelectrics, as described in Sec. II C.

B. Band structure calculations

All of our calculations are based on DFT calculations [41,42], as implemented in QUANTUM ESPRESSO [43] and using the GBRV high-throughput ultrasoft pseudopotential library [44]. We use a plane wave cutoff of 40 Ryd for band structure calculations and 45–50 Ryd for phonon calculations. For Brillouin zone integration, we use a Γ-centered grid with a density of 1500 k points per atom.

We use the PBEsol exchange-correlation functional [45], which provides more accurate lattice constants and phonon frequencies than other GGA functionals. We use the DFT+U technique [46–48], with a U value of 3 eV for transition metal d states [49], when calculating band structure related quantities. We find that for most materials this correction has a relatively minor effect beyond increasing the band gap, and larger gaps have no direct effect on thermoelectric performance as long as the gap is already large enough to avoid significant thermal carrier excitation. We perform phonon calculations using DFT perturbation theory [50] without the +U correction.

Our main results are done on fully relaxed structures with initial coordinates from the ICSD. We use PYMATGEN [51] to manipulate files from the ICSD to setup the initial structures for relaxation. Because calculations are run at a fixed number of plane waves, changes in the unit cell during relaxation can effectively modify the basis set. To ensure consistency between the basis set and the final structure, we run each relaxation three times, with a force convergence tolerance of 0.001 Ry/Bohr, an energy tolerance of 1×10^{-4} Ry, and a stress tolerance of 0.5 Kbar. For phonon calculations, we decrease the force tolerance to 5×10^{-5} Ry/Bohr. The BFGS

algorithm as implemented in QUANTUM ESPRESSO was used for relaxations.

We use maximally localized Wannier functions as implemented in WANNIER90 [52–54] to interpolate band structures and BOLTZWANN, the WANNIER90 transport module, to calculate the Seebeck coefficient and conductivity under the relaxation time approximation [55,56]. The use of Wannier interpolation allows us to perform accurate calculations of thermoelectric quantities starting from relatively sparse first-principles k-point grids, which we then interpolate to a k-point spacing of 0.02 Å^{-1}. This density is about ten times as dense as the first-principles calculation along each direction in k space. The use of Wannier functions also allows us to calculate band structure derivatives analytically, which accurately treats degenerate points in the Brillouin zone.

In order to use Wannier interpolation for this work, we had to develop a procedure for automating the construction of localized Wannier functions. Because we are interested in the properties of both valence and conduction states, we normally include all possible orbitals which could contribute to states near the Fermi level (see Supplemental Material for list). This is in contrast to many applications of Wannier functions, which are concerned with either only the occupied bands or only a localized subspace of bands (e.g., d orbitals). In these cases, the Wannier functions extend over several atoms and may be sensitive to the details of the localization procedure. For our application, we include all the relevant orbitals, which results in Wannier functions that are atomiclike and strongly localized, even before the iterative localization procedure, making the final result more robust. To calculate the Wannier functions, we use an inner "frozen" window default of 4.5 eV above and below the conduction/valence band edges in order to ensure an accurate interpolation of the band structure. In testing, our calculated thermoelectric properties are insensitive to minor variations in this window.

While the Wannierization procedure we outlined above is relatively robust, there are a few situations that can result in failures in the Wannierization, which are identified by monitoring the spread of the Wannier functions. First, if there are semicore states that were excluded from the Wannierization that overlap in energy with the valence states, it will be necessary to include those states in the valence. Second, sometimes there are problems including orbitals with high energy (e.g., Sr d states in SrTiO$_3$), as these states can become difficult to disentangle from the free electron-like bands when their energy becomes too high. In both of these cases, we simply adjust the orbitals that we include in the Wannierization procedure by hand to fix these problems. Another issue can arise if the "frozen" window overlaps with free electronlike bands. This can be fixed by adjusting this window downward to avoid overlap. We encountered all of these problematic cases only rarely, and we adjust for them when necessary.

One potential drawback of the Wannierization approach is the necessity of including a large number of empty bands in a non-self-consistent DFT calculation, in order to construct well localized conduction band Wannier functions. However, these extra bands are only required on the the sparse k-point grid, and in practice the computational cost of this step is smaller than the initial structural relaxation.

C. Thermal conductivity

For typical thermoelectrics, the thermal conductivity is dominated by the lattice thermal conductivity (κ_l). first-principles calculations of the thermal conductivity have been shown to be accurate for a wide variety of materials [58–62]. Unfortunately, these calculations require the anharmonic force constants, which are too computationally expensive to use as an initial screening tool for high-throughput calculations, especially as many of the materials we consider have large unit cells with relatively low symmetry.

There have been various recent attempts to model the lattice thermal conductivity without performing a full calculation of the anharmonic force constants [30,62–66]. Yan *et al.* use a Debye-Callaway model with a constant Gruneisen parameter [30,66]. Toher *et al.* [65] demonstrated that a modeled the Debye temperature and the Gruneisen parameter, combined using the Slack model [67,68] for thermal conductivity, is useful as a screening method for thermal conductivity. Another screening method by Bjerg *et al.* [63,69] incorporates aspects of the first-principles phonon band structure to approximate the lattice thermal conductivity.

In this work, we want a method which is both computationally feasible to apply to a few dozen compounds to use as a secondary screening procedure, and accurate enough to provide a reasonable ordering of compounds to consider for further study. We employ a method similar to the model in Bjerg *et al.*, where the Gruneisen parameter (γ) and the Debye temperature (Θ_D) are calculated from the first-principles phonon dispersion:

$$\Theta_D = n^{-1/3} \sqrt{\frac{5\hbar^2}{3k_B^2} \frac{\int_0^\infty \omega^2 g(\omega) d\omega}{\int_0^\infty g(\omega) d\omega}}, \quad (2)$$

$$\gamma^2 = \frac{\sum_i \int \frac{d\mathbf{q}}{8\pi^3} \gamma_{i\mathbf{q}}^2 C_{i\mathbf{q}}}{\sum_i \int \frac{d\mathbf{q}}{8\pi^3} C_{i\mathbf{q}}}, \quad (3)$$

$$\gamma_{i\mathbf{q}} = -\frac{V}{\omega_{i\mathbf{q}}} \frac{\partial \omega_{i\mathbf{q}}}{\partial V}, \quad (4)$$

where n is the number of atoms per unit cell, $\omega_{i\mathbf{q}}$ is the angular frequency of phonon mode i at q-point $\mathbf{q}$, $g(\omega)$ is the phonon density of states, $\gamma_{i\mathbf{q}}$ is the mode Gruneisen parameter, $C_{i\mathbf{q}}$ is the mode specific heat, and V is the volume. The sum for the Gruneisen parameter is only performed over modes with $\hbar\omega_{i\mathbf{q}} < k_B\Theta_D$. As per the discussion in Refs. [63,69], we square $\gamma_{i\mathbf{q}}$ to avoid cancellation between positive and negative anharmonicity when calculating γ.

Using the Debye temperature and Gruneisen parameter calculated above, we then insert them into the Slack model [63,67,68,70,71]:

$$\kappa_l(T) = \frac{0.849 \times 3\sqrt[3]{4}}{20\pi^3(1 - 0.514\gamma^{-1} + 0.228\gamma^{-2})}$$

$$\times \left(\frac{k_B\Theta_D}{\hbar}\right)^2 \frac{k_B M V^{\frac{1}{3}}}{\hbar\gamma^2} \frac{\Theta_D}{T}, \quad (5)$$

where M is the average atomic mass. We find that the Debye temperature and Gruneisen parameter used in this way contain almost all of the information of the full Bjerg model, as shown in Table I, which presents correlations of various models and

TABLE I. Correlations of various quantities with the reference thermal conductivities at 300 K (see Ref. [57] for list). κ_{Slack} is the model used in this work [see Eq. (5)]; Bjerg refers to the full model of Ref. [63]. Pearson and Spearman refer to the standard Pearson correlation and the Spearman rank correlation, respectively. The first two columns include all materials, the next two are limited to materials with $\kappa_l < 50$ W m^{-1} K^{-1} at 300 K.

Quantity	Pearson	Spearman	Pearson Low κ_l	Spearman Low κ_l
κ_{Slack}	0.83	0.91	0.65	0.83
Bjerg [63]	0.93	0.92	0.69	0.88
Θ_D	0.74	0.82	0.43	0.71
$1/\gamma$	0.39	0.75	0.66	0.60
Θ_D/γ	0.71	0.89	0.60	0.83

quantities with our reference set of thermal conductivities. In fact, as shown in Table I, the quantity Θ_D/γ also has a high rank correlation with the reference thermal conductivities, although there is no computational advantage in using Θ_D/γ instead of Eq. (5).

The reason we do not use the full Bjerg model is that in some cases we found difficulty in fully converging the acoustic modes for large unit cells. These modes depend on careful cancellation between all of the force constants to produce modes with zero eigenvalues at $q = \Gamma$, which is challenging to achieve numerically. This cancellation can be enforced at Γ by using the acoustic sum rule to modify the force constant matrix in various ways, but we sometimes found results which depend on how the rule was enforced. Therefore we opted to use a more computationally robust procedure appropriate for a high-throughput study by using the Slack model instead of the Bjerg model.

We find empirically in testing that using this combination of the Slack model with the Bjerg definition of the Debye temperature and Gruneisen parameter overestimates the thermal conductivity, so we report 70% of the model value, which improves the quantitative accuracy in our testing but makes no difference in a ranking of compounds for those with the lowest thermal conductivity. For materials with unstable phonon modes, we cannot calculate a Gruneisen parameter in a meaningful way using purely harmonic calculations, as the unstable modes must be stabilized anharmonically at finite temperature. Therefore we do not estimate a thermal conductivity for those compounds. In practice, we expect many materials with unstable modes at zero temperature to have low thermal conductivity due to anharmonic interactions, so the observation of unstable modes is already a useful indicator of anharmonicity. We present our calculated thermal conductivities at 300 K, even though we expect these materials to be used at higher temperatures, where the thermal conductivity will be lower.

We establish the validity of this method for screening the thermal conductivity by comparing the model with the experimental thermal conductivities of a variety simple binary semiconductors, as well as the first-principles thermal conductivities for a variety of half-Heusler compounds [62,65,67]. In addition, we compare with experimental thermal
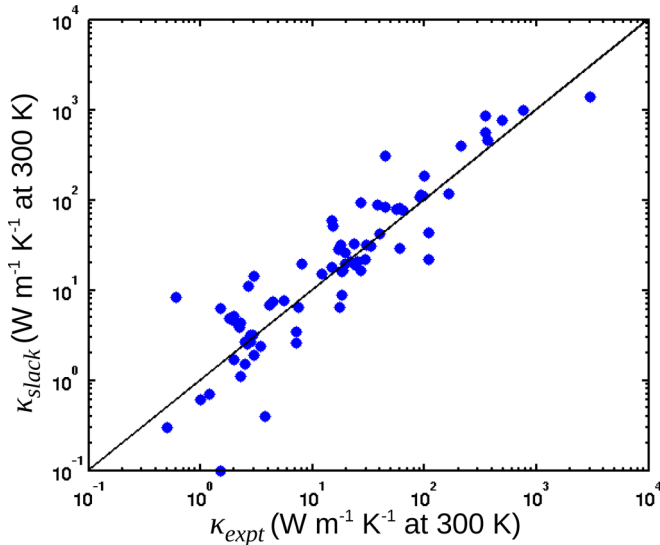
FIG. 1. Comparison of reference experimental and first-principles thermal conductivities (x axis) and the Slack model (y axis).

conductivities for a few additional oxides [72]. The results are shown graphically in Fig. 1 and correlations are given in Table I, see the Ref. [57] for details. We find that our chosen method is sufficient for screening materials for those likely to have low thermal conductivity. As shown in Table I, the Spearman rank correlation [65] between the reference and modeled thermal conductivities for the entire test set is 0.91, indicating we are able to identify promising materials. If we limit the data set to materials with $\kappa_l < 50$ W m^{-1} K^{-1} at 300 K, a more realistic range for complex oxides, the rank correlation for the full model drops to 0.83, which is still reasonable for selecting materials to study further. We also note that when considering the entire data set, the Debye temperature [see Eq. (2)] alone has a rank correlation of 0.82 with the thermal conductivity, and we make it as an initial screening tool, as it is less computationally expensive than the full model. However, directly calculating the Gruneisen parameter, rather than estimating it [30,65,66], significantly increases the accuracy of the model. Finally, experimental thermal conductivities are sensitive to many factors beyond the scope of this work, including defects and grain boundaries, which both makes comparisons with experiments difficult but increases the possibility of engineering materials to have lower thermal conductivities.

D. Effective masses

In order to understand the conductivity and Seebeck coefficient, we consider several definitions of the effective mass. Using our Wannier interpolation, we calculate derivatives of the band structure analytically [55] at the conduction band minima to find the effective mass tensor $(m_{ij})^{-1} = \frac{1}{\hbar^2}\frac{d^2E}{dk_i dk_j}$. We will sometimes concentrate on $m_{\min}$, the smallest eigenvalue of m_{ij}, which helps determine the largest value of the conductivity tensor at low temperature. We will also consider $m_{\mathrm{iso}} = (m_1 m_2 m_3)^{\frac{1}{3}}$, the isotropic effective mass, where m_1, m_2, and m_3 are the eigenvalues of m_{ij}.

A related band structure descriptor we calculate is a version of the effective mass based on the density of states (DOS) [30,73,74]:

$$m_{\mathrm{DOS}}(E) = \hbar^2 \sqrt[3]{\pi^4 g(E)g'(E)}, \qquad (6)$$

$$m_{\mathrm{DOS}}(T,n_d) = \frac{\int dE\, g(E)m_{\mathrm{DOS}}(E)\left(-\frac{df}{dE}\right)}{dE\, g(E)\left(-\frac{df}{dE}\right)}. \qquad (7)$$

In this expression, $g(E)$ is the DOS at energy E, $f(E)$ is the Fermi function, and T and n_d are the temperature and doping. This definition of m_{DOS} matches m_{eff} for a single parabolic band, but it is higher for nonparabolic bands or when multiple bands contribute to the conduction. These features allow m_{DOS} to give a good description of the Seebeck coefficient for many materials [30,73,74].

E. Materials selection and screening procedure

We are interested in discovering new n-type thermoelectric oxides, nitrides, or sulfides. As there are over 80 000 entries with oxygen in the ICSD, there is a need to significantly limit our search space before proceeding. Previous experimental and theoretical work on thermoelectrics has suggested that good thermoelectrics tend to have anisotropic and nonparabolic bands and high densities of states, all of which can be created by empty d orbitals [32,39,75–77]. Furthermore, materials with empty d orbitals can usually be doped n type, with some carriers occurring naturally due to oxygen vacancies [1–3]. Therefore, in this work, we focus on materials containing at least one of Y, Sc, Ti, Zr, Hf, Nb, Ta, Mo, or W as well as at least one of O, N, or S. In order to limit computational time, we restrict our search set to structures with primitive unit cell volumes of less than 300 Å^3.

Our screening procedure proceeds in several steps, with each step becoming more computationally expensive. First, we calculate the band gap of all our our starting materials (766 compounds) and eliminate the metals. For materials with a gap (592 materials), we calculate the Seebeck coefficient S and electronic conductivity σ/τ_e. For materials with a high power factor (191 materials), we then calculate the Debye temperature using Eq. (2). Finally, for a subset of 19 materials with high power factor and/or low Debye temperature, we calculate $\kappa_l^{\mathrm{Slack}}$ with Eq. (5). Results are presented in Table II with further details in the Ref. [57].

III. RESULTS AND DISCUSSION

We performed our screening procedure starting with 766 compounds from the ICSD as discussed in Sec. II E, consisting of 661 oxides, 60 nitrides, and 71 sulfides (some compounds contain multiple anions). Of that list, we find 592 materials with band gaps according to DFT+U (551 oxides, 53 nitrides, and 25 sulfides). For these materials, we calculate S and σ/τ_e for a variety of temperatures and dopings.

If we sort this list of candidate materials by estimated power factor, $S^2\sigma/\tau_e$, at 700 K and with optimized doping, we rediscover several compounds that have previously been measured to have good n-type thermoelectric properties. For example, doped TiO_2, $SrTiO_3$, $KTaO_3$, and TiS_2 have all

TABLE II. Thermoelectric properties of the most promising compounds. The first five columns consist of the compound name, its space group number, the DFT+U band gap (eV), the isotropic effective mass. The next several columns are the DOS, m_{DOS} [see Eqs. (6) and (7)], S, and σ/τ_e, all evaluated at 700 K and fixed 10^{21} cm^{-3} doping. The next column is $S^2\sigma/\tau_e$ at the optimized doping and at 700 K, and following column is that optimized doping. The last column is the modeled lattice thermal conductivity at 300 K. Materials with - as κ_l have unstable phonon modes or we were unable to converge the Gruneisen parameter.

Material	Space Grp.	Band Gap (eV)	m_{iso}	DOS (10^3 eV^{-1} Å^{-3})	m_{DOS}	S ($\mu V/K$)	σ/τ_e 10^{-3} $\frac{S}{m\,fs}$	$S^2\sigma/\tau_e$ 10^3 $\frac{W}{m\,K^2\,fs}$	Opt. Doping (10^{21} cm^{-3})	κ_l $\frac{W}{mK}$
CaTaAlO$_5$	15	4.0	2.8	4.08	5.0	−189	42.9	1.7	3	—
TiO$_2$	225	1.7	1.1	1.53	17.0	−305	9.6	1.7	8	—
LiNbO$_3$	161	3.5	2.1	3.92	7.0	−245	23.4	1.6	2	40
TiO$_2$	136	2.1	2.2	3.63	7.5	−250	20.7	1.6	3	<1
HfS$_2$	164	1.6	1.6	5.51	2.7	−165	56.9	1.5	1	3.4
NaNbO$_3$	63	1.8	3.8	1.89	0.8	−268	75.6	1.4	4	—
Ba$_2$TaInO$_6$	225	4.3	2.3	2.75	10.0	−285	12	1.4	5	—
YClO	129	5.1	1.1	3.20	6.6	−182	32.2	1.4	3	6.0
LiTaO$_3$	161	3.8	2.9	5.50	3.4	−204	36.3	1.4	1	34
Li$_2$ZrN$_2$	164	1.9	0.6	5.10	3.5	−178	42.5	1.4	2	19
CaTiSiO$_5$	15	3.2	4.0	4.28	6.4	−229	25.5	1.3	2	1.1
HgWO$_4$	15	2.4	1.5	4.22	3.5	−171	46.5	1.3	2	—
P$_2$WO$_8$	12	2.3	11.8	6.01	3.5	−150	56.1	1.3	0.7	6.5
ZrS$_2$	164	1.1	1.6	4.88	3.3	−172	45.1	1.3	2	22
TaPO$_5$	85	3.7	2.6	4.38	4.1	−160	49.5	1.3	2	—
LaTaO$_4$	36	3.4	2.9	5.13	3.7	−183	38.1	1.3	2	26
NbTl$_3$S$_4$	217	2.3	0.9	3.59	8.6	−246	19.2	1.3	2	—
SrTaNO$_2$	140	0.9	0.7	3.31	1.8	−109	122.6	1.3	0.3	—
TiS$_2$	164	0.4	0.4	4.73	3.7	−171	42	1.3	2	5.3
PbTiO$_3$	99	2.0	0.6	3.68	1.7	−489	35.3	1.2	7	16
Sr$_2$TaInO$_6$	225	4.3	2.1	2.65	10.0	−266	10.4	1.2	6	—
SrTiO$_3$	140	1.2	1.3	3.56	1.6	−165	39.5	1.2	6	—
NaNbN$_2$	166	1.1	0.8	3.70	3.3	−142	42	1.1	4	—
HfTaNO$_3$	25	2.0	0.8	4.22	2.4	−122	73	1.1	0.6	—
KNbO$_3$	99	1.6	3.0	1.82	1.3	−367	75.5	1.1	3	—
HfSiO$_4$	141	5.8	2.7	4.36	6.3	−276	18.8	1.1	2	190
Y$_2$O$_3$	164	4.2	1.0	3.44	3.7	−122	41.8	1.1	4	5.8
ZrO$_2$	225	3.7	1.1	3.78	4.6	−145	18.7	1.1	10	—
CdTiO$_3$	62	2.5	1.0	5.2	4.4	−205	20.7	0.9	2	<1
CaTiO$_3$	62	2.7	1.1	5.23	3.5	−170	26.8	0.8	1	<1
Y$_2$Ti$_2$O$_7$	227	3.1	1.1	2.21	10.7	−224	11.4	0.6	2	<1

been measured to have promising power factors and show up highly in our list [1–3,9,10,32,34,78–81]. This gives us confidence that our screening procedure is useful. In addition to these previously measured materials, there are a variety of compounds that have not been studied for thermoelectric applications and which may have properties that are superior to existing materials. In Table II, we list some of our most promising candidate materials, including those with high $S^2\sigma/\tau_e$ and a few with moderate $S^2\sigma/\tau_e$ and low κ_l. We remove structures that are minor distortions of other structures on the list, that have missing atoms in the ICSD, or that are only theoretically proposaled structures; full results are presented in the Ref. [57].

We begin our analysis by looking for patterns in the entire data set. First, we note that under the rigid band model used in this work, most materials have optimal dopings of about 10^{21} cm^{-3}, which corresponds to dopings on the order to 10%. While this is much higher than typical semiconductor thermoelectrics, it is consistent with the behavior of oxides like SrTiO$_3$ [1–3,9,10]. Reaching such high doping values may be

difficult in practice and will require further experimental and theoretical work (see, for instance, Ref. [82]). In this work, we concentrate on identifying promising materials for further optimization.

In Fig. 2, we plot the values of S versus σ/τ_e, at 700 K and for a fixed doping of 10^{21} cm^{-3}. The color scale shows the value of $S^2\sigma/\tau_e$ [83]. There is a clear trade-off between S and σ/τ_e, which is consistent with the behavior of simple parabolic bands where $S \propto m_{\rm eff}$ and $\sigma \propto 1/m_{\rm eff}$, where $m_{\rm eff}$ is the effective mass [4]. The best materials do not maximize either S or σ/τ_e, but instead have S and σ/τ_e values in the center of observed range, but with a larger combination than is typical. In the following sections, we explore in more detail how some of these individual materials achieve this higher than expected combination of S and σ/τ_e.

The trade-off between S and σ/τ_e makes finding a simple descriptor of the power factor in terms of features of the band structure very difficult, even though we can relate σ and S individually to features in the band structure. In Table III, we present Spearman rank correlations between
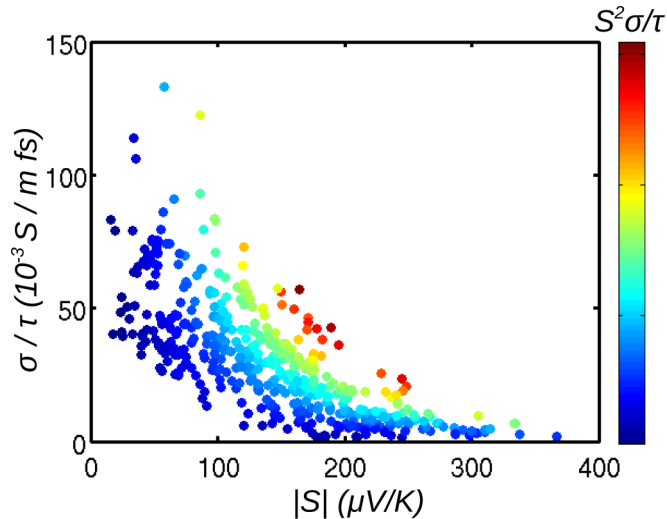
FIG. 2. $|S|$ [μV/K] vs σ/τ_e [$\times 10^3 \frac{S}{m\,fs}$] for the entire data set, at $T = 700$ K and doping at 10^{21} cm^{-3}. The color scale indicates size of power factor, $S^2\sigma/\tau_e$.
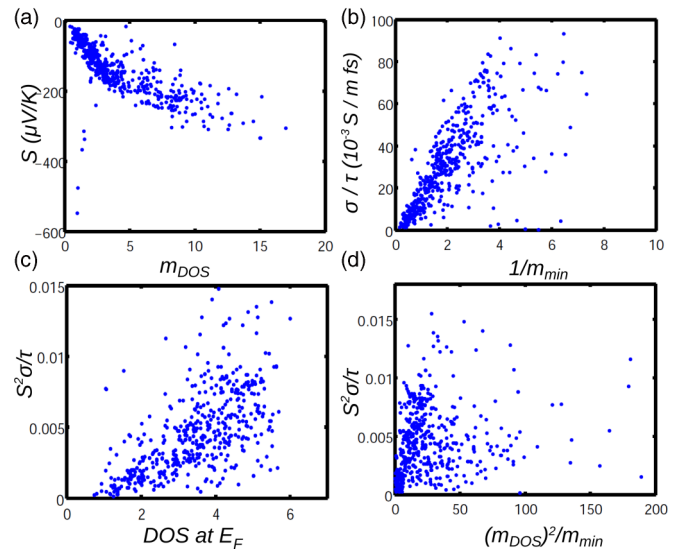

FIG. 3. Thermoelectric properties of the entire data set, at fixed $T = 700$ K $n_d = 10^{21}$ cm^{-3}. (a) m_{DOS} vs S, (b) $1/m_{min}$ vs σ/τ_e, where m_{min} is the smallest component of m_{ij}, (c) DOS at E_F vs the power factor, and (d) m_{DOS}^2/m_{min} vs the power factor.

several thermoelectric properties and various descriptors of the band structure, and several of these relationships are plotted in Fig. 3.

For example, we find that the smallest value of the effective mass tensor, m_{min}, is highly correlated with σ/τ_e, and we plot this relationship in Fig. 3(b). Unsurprisingly, materials with small effective masses usually have high conductivities, although this relationship can be complicated by anisotropy in the effective mass tensor or by many bands contributing to the conduction. Similarly, as shown in Fig. 3(a), we find that we can model the Seebeck coefficient as $S \propto m_{DOS}(T, n_d)$ [see Eq. (7)].

Despite these relatively strong relationships for S and σ in terms of certain definitions of the effective mass, we find that the combination of m_{DOS}^2/m_{min} has only a weak correlation with $S^2\sigma/\tau_e$, as plotted in Fig. 3(d). The problem is that as shown in Table III, the two definitions of the effective mass are strongly correlated with each other, and dividing one by another does not produce a useful descriptor. Other

quantities like m_{iso} have similar problems. Furthermore, all of the effective masses, as well as S and σ/τ_e, are strongly correlated or anticorrelated with each other, but none are by themselves strongly correlated with the power factor. This can be understood in part by looking at Fig. 2, which shows that the best materials do not lie at the extreme of either S or σ/τ_e, but they instead have an atypical relationship between S and σ/τ_e. Finding a simple descriptor of that relationship is difficult when the stronger trend is the trade-off between S and σ/τ_e. In addition, in many anisotropic materials, the Seebeck coefficient and conductivity are not maximized in the same direction, which makes finding a simple descriptor for the maximum power factor more difficult. Finally, as we will see below, all of our best materials have unusual band structures with some combination of high anisotropy, nonparabolic behavior, and multiple bands contributing to the conduction, and identifying these qualities requires going beyond a simple effective mass description of parabolic bands.

The best simple descriptor we found for $S^2\sigma/\tau_e$ does not include any effective mass, but instead is just the DOS evaluated at the relevant doping and temperature, as shown in Fig. 3(c). While there is a clear relationship between the DOS and the power factor, many high DOS materials have low power factors, making a high DOS a useful design criterion but not a sufficient condition for good thermoelectric performance.

In the following subsections, we will investigate the band structures of some of the materials in Table II, in order to evaluate the mechanisms that allow these particular materials to minimize the trade-off between S and σ. We find that these materials separate roughly into three classes of materials, although some materials fall into several classes. In general, the mechanisms for high power factors consist of combining a large number of flat bands near the conduction band minimum with at least some highly dispersive bands. This combination allows a large number of carriers, some of which are in

TABLE III. Spearman rank correlation matrix of various band structure descriptors and thermoelectric quantities at 700 K and at a fixed doping of 10^{21} cm^{-3}. $S^2\sigma/\tau_e$ is the power factor, $|S|$ is the absolute value of the Seebeck coefficient, σ/τ_e is the electrical conductivity, m_{min} is the minimum value of m_{ij}, the effective mass tensor, m_{DOS} is defined in Eq. (7), and DOS is the density of states at the Fermi level. Correlations with absolute value above 0.65 are in bold.

Quantity	$S^2\sigma/\tau_e$	$|S|$	σ/τ_e	m_{min}	m_{DOS}	DOS
$S^2\sigma/\tau_e$	—	0.44	0.07	−0.03	0.22	**0.67**
$|S|$	0.44	—	**−0.81**	**0.66**	**0.84**	0.43
σ/τ_e	0.07	**−0.81**	—	**−0.81**	**−0.83**	−0.21
m_{min}	−0.03	**0.66**	**−0.81**	—	**0.74**	0.28
m_{DOS}	0.22	**0.84**	**−0.83**	**0.74**	—	0.32
DOS	**0.67**	0.43	−0.21	0.28	0.32	—

dispersive bands, increasing σ, while at the same time keeping the Fermi level near the conduction band minimum, where $|S|$ is largest, mitigating the typical trade-off.

A. Symmetry driven degeneracy

This group of promising thermoelectrics contains materials that have symmetries (or near symmetries) which cause degeneracies in the conduction band minimum. This degeneracy increases the DOS for any given Fermi level, relative to a material without degeneracies. These degeneracies can be due to a single degenerate minimum in Brillouin zone, or they can be due to a band structure with a conduction band minimum which is repeated due to symmetry.

In addition to having degeneracies, the conduction bands of these materials all consist of empty transition metal d orbitals that have highly anisotropic dispersions [32,34,39,77]. These anisotropic band structures allow the material to have both low m_{eff} and high m_{eff} bands at the same minimum, combining large Seebeck coefficients with the high conductivity. Similar degeneracies and anisotropic bands are behind the high power factors of several semiconducting materials, which rely of empty p orbitals instead of empty d orbitals [26,30,39,77].

All of these features are present in the band structure of cubic SrTiO$_3$, as shown in see Fig. 4, which is known to be a good n-type thermoelectric. SrTiO$_3$ has a single triply degenerate conduction band minimum at Γ due to the t_{2g} states originating from the Ti-d orbitals. These bands have highly anisotropic dispersions, with one nearly flat band ($m_{\mathrm{eff}} = 6.3$) and two highly dispersive bands ($m_{\mathrm{eff}} = 0.4$) going from Γ to X. The combination of high degeneracy and high effective mass bands with very low effective mass bands, which allow for high conductivity, is what allows SrTiO$_3$ to escape the normal trade-off between S and σ/τ_e.

Similar features are present in many of the other perovskite variants which we find to be candidate thermoelectrics (SrTiO$_3$, PbTiO$_3$, NaNbO$_3$, LiNbO$_3$, KNbO$_3$, LiTaO$_3$, Ba$_2$TaInO$_6$, CaTiO$_3$, Sr$_2$TaInO$_6$, SrTaNO$_2$). In addition, various phases of TiO$_2$ and ZrO$_2$ have similar features which lead to high power factors. Many of these materials have been studied as thermoelectrics before, and the mechanisms leading to their power factors are relatively well-known
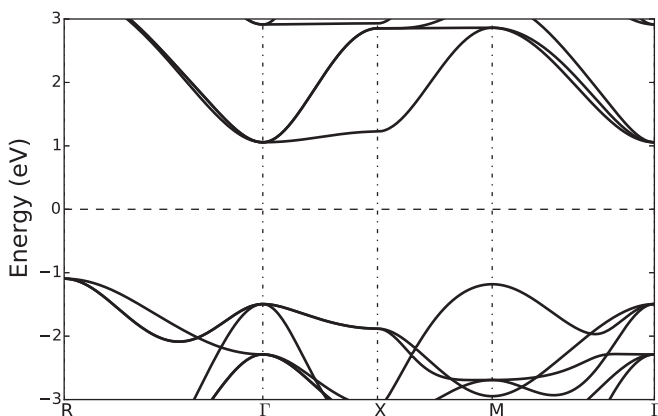
[26,30,32,34], so we will proceed with a discussion of the next two groups.

B. Low-dimensional conductors

While all of the structures studied in this work are three-dimensional, in many cases, the atoms, which dominate the conduction band minima, are arranged in two-dimensional layers, one-dimensional lines, or zero-dimensional dots, which leads to effectively low-dimensional conduction. In some cases, the material itself consists of weakly bound layers, while in others, there are strong bonds in all three directions, but the transition metals are arranged in a low-dimensional way.

Reducing the effective dimensionality of a material results in highly anisotropic conduction bands and an increased DOS at the bottom of bands, which can increase the power factor [76,77,84]. The idea of improving the power factor of a candidate thermoelectric by reducing its dimensionality and therefore increasing its DOS is well-known, and has been shown in SrTiO$_3$ superlattices [75,84]. We note that here we are considering thermodynamically stable materials, rather than artificial superlattices, nanowires, or quantum dots, which should reduce manufacturing costs and increase thermodynamic stability.

We present two examples of effectively low-dimensional materials, which we predict have high power factors. First, in Fig. 5, we show the band structure and atomic structure of HfS$_2$, which consists of weakly bound two-dimensional hexagonal trilayers. The conduction bands are very flat from M to the minimum at L ($m_{\mathrm{eff}} = 4.5$), characteristic of two-dimensional materials, but they are much more dispersive in other directions ($m_{\mathrm{eff}} = 0.3$).

Second, in Fig. 6, we show the band structure and atomic structure of CaTaAlO$_5$, which consists of TaO$_6$ octahedra

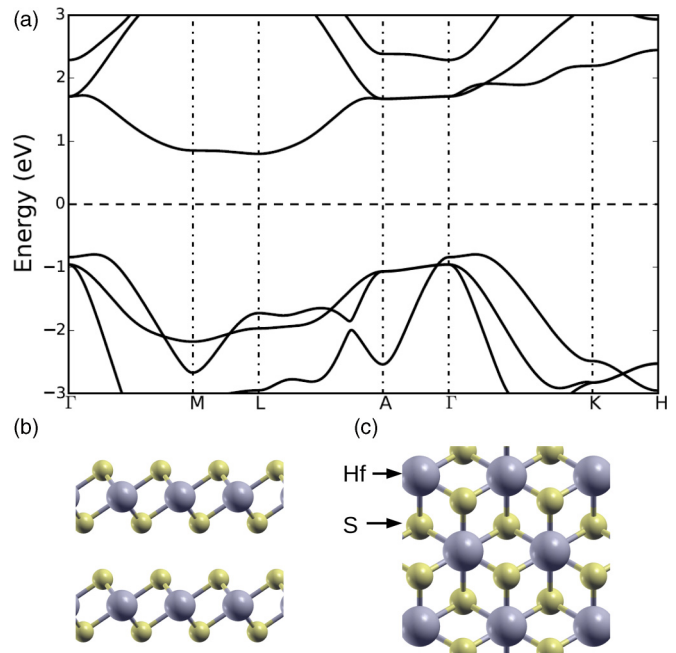FIG. 4. Band structure of cubic SrTiO$_3$. Energies are relative to the Fermi level.

FIG. 5. (a) Band structure of HfS$_2$. (b) and (c) Side and top views of HfS$_S$. Larger gray atoms are Hf, smaller yellow atoms are S.

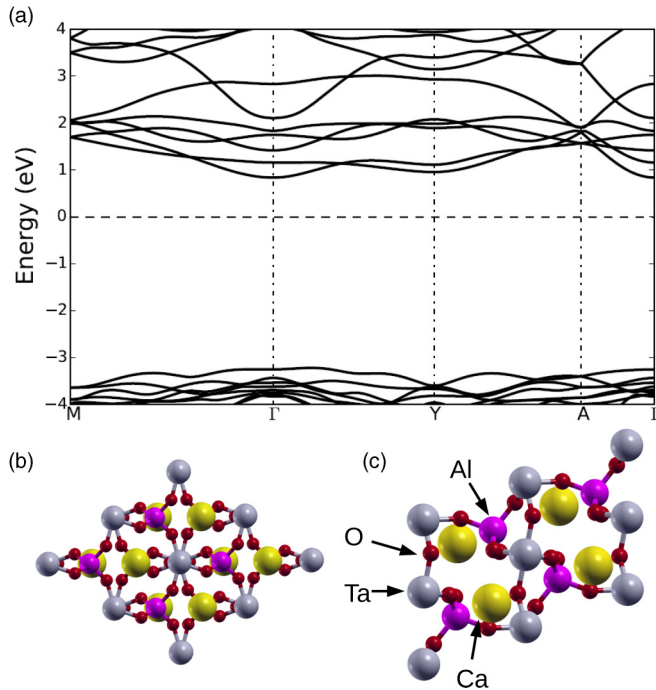FIG. 7. Band structure of Sr_2TaInO_6. Bands with greater then 35% In content are colored red, others are black.

FIG. 6. (a) Band structure of $CaTaAlO_5$. (b) and (c) Top and side views of $CaTaAlO_5$. Large yellow atoms are Ca, medium gray atoms are Ta, smaller magenta atoms are Al, smallest red atoms are O.

arranged into one-dimensional columns that are separated from each other by Ca ions and AlO_4 tetrahedra. This arrangement of Ta atoms leads to an anisotropic band structure with very flat bands from Γ to Y ($m_{eff} = 2.4$) but stronger dispersion from Γ to A ($m_{eff} = 0.5$). There are additional nearly degenerate conduction band minima at Y, which also contribute to the DOS. In HfS and $CaTaAlO_5$, the high DOS and the strong anisotropy, which are caused by the low dimensionality, create the conditions for a high power factor.

Within our set of candidate thermoelectrics, ZrS_2, TiS_2, HfS_2, YClO, $CaTiSiO_5$, WP_2O_8, $TaPO_5$, $NaNbN_2$ have quasi-two-dimensional structures, $CaTaAlO_5$, $HgWO_4$, $LaTaO_4$, and $HfSiO_4$ have quasi-one-dimensional structures, and $NbTl_3S_4$, Ba_2TaInO_6, and Sr_2TaInO_6 have quasi-zero-dimensional structures, as their transition metals are separated from each other.

There are other possible advantages in using low-dimensional materials as thermoelectrics besides the increased DOS, including potentially lower thermal conductivity, due to phonon scattering from the atomic layers, as well as the ability to physically separate dopants from conducting channels, which can reduce electron scattering. One disadvantage is that the thermoelectric properties of low-dimensional materials will be anisotropic, resulting in reduced efficiency in polycrystalline samples.

C. Accidental degeneracies

One final mechanism for increasing the power factor of an n-type oxide is to find or engineer a material with accidental degeneracies of the conduction band minimum. While this can happen for physically similar bands which happen to be
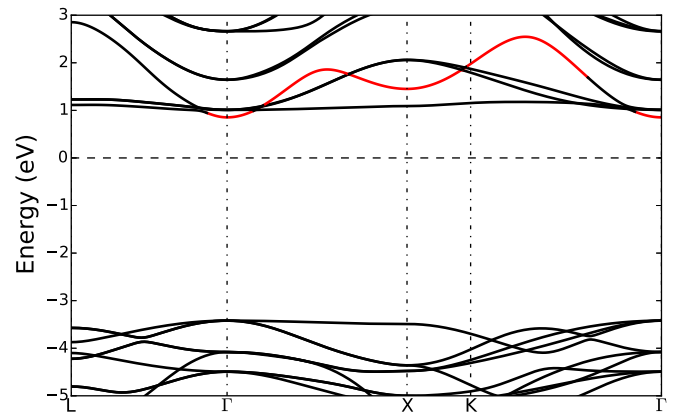
degenerate at different points in the Brillouin zone, here we consider cases where the bands come from different orbitals and have different effective masses. For example, in the double perovskite Sr_2TaInO_6, the conduction band consists of both Ta d states and In p states, which happen to be at similar energies (see Fig. 7, which highlights the In states in red). The In states have low effective masses ($m_{eff} = 0.2$–0.3), while the Ta states have much higher effective masses ($m_{eff} = 13$–62), allowing the material to take advantage of both types of bands, in addition to the increased DOS provided by the near degeneracy. The large effective masses of the Ta-d bands are caused by small overlap between them and many of the neighboring In-p orbitals, which results in very flat bands, which contribute to a high DOS and high power factor.

Similar materials with two different atoms contributing to the conduction are $HgWO_4$, Ba_2TaInO_6, and $NbTl_3S_4$, where the Hg($+2$), In($+3$), and Tl($+1$) ions, contribute empty s/p bands at similar energies to the transition metal d bands. In addition, in both YClO and Y_2O_3, the empty s and d states of the Y atoms are both located near the conduction band minimum, which results in similar behavior to the case where the orbitals come from different atoms. Depending on the crystal structure and the anions, it may be possible to engineer empty s bands from Cu, Zn, Ag, Cd, Au, or Hg or p bands from In, Sn, Tl, Pb, or Bi to become degenerate with transition metal bands in this fashion [85]. This type of engineering could allow one material to take advantage of the high Seebeck coefficients of transition metal oxides while incorporating the higher mobility of semiconductors, which often have empty s or p orbitals from main group elements. The exact alignments of empty states from different atoms is difficult to predict using DFT$+U$, so further study of these materials to determine the band alignments more precisely may be necessary.

D. Thermal conductivity

Due to the high computational cost, we were not able to calculate the thermal conductivity of our full data set. For 191 compounds, we calculated the Debye temperature [see Eq. (2)], which is fairly strongly correlated with thermal conductivity (see Table I and Ref. [57]). Calculations of the Debye temperature are both less sensitive to the q-point

sampling of the phonon band structure than the Gruneisen parameter and require the phonons at only one volume, making the computations much faster.

We find that in our set of transition metal oxides, nitrides, and sulfides, there is relatively little variation in the Debye temperature (mean of 342 K, standard deviation of 66 K), as compared to our test data set of simple binary and ternary semiconductors (mean 319 K, standard deviation 234 K). This is likely due to the fact that all of our compounds contain ionic bonds between light anions and medium to heavy transition metals, while the test data set contains a range of bonds, from covalent to ionic, and a range of atom masses. In both data sets, there is a significant correlation between V^{-1} and the Debye temperature, with a correlation coefficient of 0.68 in the oxides, and 0.88 in the test set. This suggests that looking at oxides with larger unit cells could be beneficial [30,66].

Due to the relatively weak variation in the Debye temperature throughout our set of oxides, the Gruneisen parameter becomes more important to identify the materials likely to have low thermal conductivity. Many of the oxides we consider have soft or unstable phonon modes, which likely results in strong anharmonicity and low thermal conductivity, but this is difficult to quantify without more involved calculations. Due to the large computational cost, we are only able to calculate the Gruneisen parameter of the materials in Table II. We do not have a large enough database of oxide Gruneisen parameters to identify any trends that would predict which materials will have soft modes without doing phonon calculations.

As shown in Table II, many of the materials we have identified as having promising power factors also have low thermal conductivity according to our model. Most of the perovskite materials we study have strongly anharmonic modes, which leads to relatively low thermal conductivities, both in our calculations and in experiment [72]. In addition, we find that many of the materials with one or two-dimensional

bonding also have soft modes, likely due to the fact that many of the atoms are relatively free to vibrate in at least one direction.

IV. CONCLUSIONS

We have used high throughput first-principles calculations to search for *n*-type transition metal oxides, nitrides, and sulfides which are promising for thermoelectric applications. We find many materials with estimated power factors, which are comparable to or surpass previously studied oxide thermoelectrics.

Across the entire sample of compounds, we find the expected correlations between the Seebeck coeffient and electrical conductivity with the effective mass and inverse effective mass, respectively, of the conduction band electrons. However, to find materials with high power factors, it is necessary to look for materials which are not well described by a single parabolic band, but instead have degeneracy, anisotropy, or other features which result in a high density of states combined with dispersive bands at the Fermi level. These materials achieve their high power factors due to some combination of symmetry-enforced degeneracies, low dimensionality, or accidental degeneracies. In addition, we use phonon calculations to model the thermal conductivity of our best candidates, and we find many that have low lattice thermal conductivity or that require anharmonic stabilization of the harmonic modes. We hope further work on these materials, as well as the understanding gained by examining the mechanisms which lead to high power factors in oxides, will lead to improved thermoelectric performance in oxides.

[1] S. Walia, S. Balendhran, H. Nili, S. Zhuiykov, G. Rosengarten, Q. Wang, M. Bhaskaran, S. Sriram, M. Strano, and K. Kalantar-zadeh, Prog. Mat. Sci. **58**, 1443 (2013).

[2] M. Backhaus-Ricoult, J. Rustad, L. Moore, C. Smith, and J. Brown, Appl. Phys. A **116**, 433 (2014).

[3] J. He, Y. Liu, and R. Funahashi, J. Mater. Res. **26**, 1762 (2011).

[4] M. Zebarjadi, K. Esfarjani, M. S. Dresselhaus, Z. F. Ren, and G. Chen, Energy Environ. Sci. **5**, 5147 (2012).

[5] S. Riffat and X. Ma, Appl. Therm. Eng. **23**, 913 (2003).

[6] M. W. Gaultois, T. D. Sparks, C. K. H. Borg, R. Seshadri, W. D. Bonificio, and D. R. Clarke, Chem. Mater. **25**, 2911 (2013).

[7] I. Terasaki, Y. Sasago, and K. Uchinokura, Phys. Rev. B **56**, R12685 (1997).

[8] M. Ohtaki, T. Tsubota, K. Eguchi, and H. Arai, J. Appl. Phys. **79**, 1816 (1996).

[9] S. Ohta, T. Nomura, H. Ohta, M. Hirano, H. Hosono, and K. Koumoto, Appl. Phys. Lett. **87**, 092108 (2005).

[10] T. Okuda, K. Nakanishi, S. Miyasaka, and Y. Tokura, Phys. Rev. B **63**, 113104 (2001).

[11] W. Pan, S. Phillpot, C. Wan, A. Chernatynskiy, and Z. Qu, MRS Bull. **37**, 917 (2012).

[12] A. Jain, G. Hautier, C. J. Moore, S. P. Ong, C. C. Fischer, T. Mueller, K. A. Persson, and G. Ceder, Comput. Mater. Sci. **50**, 2295 (2011).

[13] G. Ceder, Y. Chiang, D. Sadoway, M. Aydinol, Y. Jang, and B. Huang, Nature (London) **392**, 694 (1998).

[14] A. R. Akbarzadeh, V. Ozolins, and C. Wolverton, Adv. Mater. **19**, 3233 (2007).

[15] D. Morgan, G. Ceder, and S. Curtarolo, Meas. Sci. Technol. **16**, 296 (2005).

[16] O. Levy, G. L. W. Hart, and S. Curtarolo, J. Am. Chem. Soc. **132**, 4830 (2010).

[17] G. H. Johannesson, T. Bligaard, A. V. Ruban, H. L. Skriver, K. W. Jacobsen, and J. K. Norskov, Phys. Rev. Lett. **88**, 255506 (2002).

[18] S. Curtarolo, D. Morgan, and G. Ceder, Calphad **29**, 163 (2005).

[19] W. Setyawana and S. Curtarolo, Comput. Mater. Sci. **49**, 299 (2010).

[20] X. Zhang, L. Yu, A. Zakutayev, and A. Zunger, Adv. Funct. Mater. **22**, 1425 (2012).

[21] J. W. Bennett and K. M. Rabe, J. Solid State Chem. **195**, 21 (2012).

[22] S. Curtarolo, G. Hart, M. Buongiorno Nardelli, N. Mingo, S. Sanvito, and O. Levy, Nat. Mater. **12**, 191 (2013).

[23] A. Belsky, M. Hellenbrandt, V. L. Karen, and P. Luksch, Acta Crystallogr. Sect. B **58**, 364 (2002).

[24] S. Wang, Z. Wang, W. Setyawan, N. Mingo, and S. Curtarolo, Phys. Rev. X **1**, 021012 (2011).

[25] I. Opahle, A. Parma, E. J. McEniry, R. Drautz, and G. K. Madsen, New J. Phys. **15**, 105010 (2013).

[26] P. Gorai, P. Parilla, E. S. Toberer, and V. Stevanovi, Chem. Mater. **27**, 6213 (2015).

[27] Q. Hao, H. Zhao, and N. Lu, in *Symposium H Mechanics of Energy Storage and Conversion Batteries, Thermoelectrics and Fuel Cells*, MRS Symposia Proceedings No. 1774 (Materials Research Society, Pittsburgh, 2015), p. 25.

[28] Q. Hao and H. Zhao, ECS Trans. **69**, 11 (2015).

[29] T. D. Sparks, M. W. Gaultois, A. Oliynyk, J. Brgoch, and B. Meredig, Scr. Mater. **111**, 10 (2016).

[30] J. Yan, P. Gorai, B. Ortiz, S. Miller, S. A. Barnett, T. Mason, V. Stevanovic, and E. S. Toberer, Energy Environ. Sci. **8**, 983 (2015).

[31] D. Singh and D. Kasinathan, J. Electron. Mater. **36**, 736 (2007).

[32] K. Shirai and K. Yamanaka, J. Appl. Phys. **113**, 053705 (2013).

[33] G. K. H. Madsen, K. Schwarz, P. Blaha, and D. J. Singh, Phys. Rev. B **68**, 125212 (2003).

[34] H. Usui, S. Shibata, and K. Kuroki, Phys. Rev. B **81**, 205121 (2010).

[35] G. K. H. Madsen, J. Am. Chem. Soc. **128**, 12140 (2006).

[36] J. Ziman, *Principles of the Theory of Solids* (Cambridge University Press, Cambridge, 1972).

[37] B. Qiu, Z. Tian, A. Vallabhaneni, B. Liao, J. M. Mendoza, O. D. Restrepo, X. Ruan, and G. Chen, Europhys. Lett. **109**, 57006 (2015).

[38] N. A. Deskins and M. Dupuis, Phys. Rev. B **75**, 195212 (2007).

[39] X. Chen, D. Parker, and D. J. Singh, Sci. Rep. **3**, 3168 (2013).

[40] K. P. Ong, D. J. Singh, and P. Wu, Phys. Rev. B **83**, 115110 (2011).

[41] P. Hohenberg and W. Kohn, Phys. Rev. **136**, B864 (1964).

[42] W. Kohn and L. Sham, Phys. Rev. **140**, A1133 (1965).

[43] P. Giannozzi *et al.*, J. Phys.: Condens. Matter **21**, 395502 (2009).

[44] K. F. Garrity, J. W. Bennett, K. M. Rabe, and D. Vanderbilt, Comput. Mater. Sci. **81**, 446 (2014).

[45] J. P. Perdew, A. Ruzsinszky, G. I. Csonka, O. A. Vydrov, G. E. Scuseria, L. A. Constantin, X. Zhou, and K. Burke, Phys. Rev. Lett. **100**, 136406 (2008).

[46] V. I. Anisimov, J. Zaanen, and O. K. Andersen, Phys. Rev. B **44**, 943 (1991).

[47] S. L. Dudarev, G. A. Botton, S. Y. Savrasov, C. J. Humphreys, and A. P. Sutton, Phys. Rev. B **57**, 1505 (1998).

[48] M. Cococcioni and S. de Gironcoli, Phys. Rev. B **71**, 035105 (2005).

[49] V. Stevanović, S. Lany, X. Zhang, and A. Zunger, Phys. Rev. B **85**, 115104 (2012).

[50] S. Baroni, S. de Gironcoli, A. Dal Corso, and P. Giannozzi, Rev. Mod. Phys. **73**, 515 (2001).

[51] S. P. Ong, W. D. Richards, A. Jain, G. Hautier, M. Kocher, S. Cholia, D. Gunter, V. L. Chevrier, K. A. Persson, and G. Ceder, Comput. Mater. Sci. **68**, 314 (2013).

[52] N. Marzari and D. Vanderbilt, Phys. Rev. B **56**, 12847 (1997).

[53] I. Souza, N. Marzari, and D. Vanderbilt, Phys. Rev. B **65**, 035109 (2001).

[54] A. A. Mostofi, J. R. Yates, Y.-S. Lee, I. Souza, D. Vanderbilt, and N. Marzari, Comput. Phys. Commun. **178**, 685 (2008).

[55] J. R. Yates, X. Wang, D. Vanderbilt, and I. Souza, Phys. Rev. B **75**, 195121 (2007).

[56] G. Pizzi, D. Volja, B. Kozinsky, M. Fornari, and N. Marzari, Comput. Phys. Commun. **185**, 422 (2014).

[57] See Supplemental Material at http://link.aps.org/supplemental/10.1103/PhysRevB.94.045122 for details of Wannierization procedure, thermal conductivity testing data, and thermoelectric results for the full set of materials.

[58] D. A. Broido, M. Malorny, G. Birner, N. Mingo, and D. A. Stewart, Appl. Phys. Lett. **91**, 231922 (2007).

[59] K. Esfarjani, G. Chen, and H. T. Stokes, Phys. Rev. B **84**, 085204 (2011).

[60] L. Lindsay, D. A. Broido, and T. L. Reinecke, Phys. Rev. B **87**, 165201 (2013).

[61] A. Togo, L. Chaput, and I. Tanaka, Phys. Rev. B **91**, 094306 (2015).

[62] J. Carrete, W. Li, N. Mingo, S. Wang, and S. Curtarolo, Phys. Rev. X **4**, 011019 (2014).

[63] L. Bjerg, B. B. Iversen, and G. K. H. Madsen, Phys. Rev. B **89**, 024304 (2014).

[64] A. Seko, A. Togo, H. Hayashi, K. Tsuda, L. Chaput, and I. Tanaka, Phys. Rev. Lett. **115**, 205901 (2015).

[65] C. Toher, J. J. Plata, O. Levy, M. de Jong, M. Asta, M. B. Nardelli, and S. Curtarolo, Phys. Rev. B **90**, 174107 (2014).

[66] E. S. Toberer, A. Zevalkink, and G. J. Snyder, J. Mater. Chem. **21**, 15843 (2011).

[67] G. A. Slack, *Solid State Physics* (Academic, New York, 1979), Vol. 34, Chap. 1, p. 1.

[68] G. Leibfried and E. Schlomann, Nachr. Akad. Wiss. Goettingen, Math.-Phys., Kl. 2A: Math.-Phys.-Chem. Abt **4**, 71 (1954).

[69] G. K. H. Madsen, A. Katre, and C. Bera, Phys. Status Solidi A **213**, 802 (2016).

[70] D. T. Morelli, J. P. Heremans, and G. A. Slack, Phys. Rev. B **66**, 195304 (2002).

[71] G. A. Slack and S. Galginaitis, Phys. Rev. **133**, A253 (1964).

[72] M. Tachibana, T. Kolodiazhnyi, and E. Takayama-Muromachi, Appl. Phys. Lett. **93**, 092902 (2008).

[73] K. Kutorasinski, B. Wiendlocha, J. Tobola, and S. Kaprzyk, Phys. Rev. B **89**, 115205 (2014).

[74] K. Kutorasinski, B. Wiendlocha, S. Kaprzyk, and J. Tobola, Phys. Rev. B **91**, 205201 (2015).

[75] H. Ohta, S. Kim, Y. Mune, T. Mizoguchi, K. Nomura, S. Ohta, T. Nomura, Y. Nakanishi, Y. Ikuhara, M. Hirano *et al.*, Nat. Mater. **6**, 129 (2007).

[76] M. Dresselhaus, G. Chen, M. Tang, R. Yang, H. Lee, D. Wang, Z. Ren, J.-P. Fleurial, and P. Gogna, Adv. Mater. **19**, 1043 (2007).

[77] D. Parker, X. Chen, and D. J. Singh, Phys. Rev. Lett. **110**, 146601 (2013).

[78] H. Imai, Y. Shimakawa, and Y. Kubo, Phys. Rev. B **64**, 241104 (2001).

[79] A. Sakai, T. Kanno, S. Yotsuhashi, H. Adachi, and Y. Tokura, Jpn. J. Appl. Phys. **48**, 097002 (2009).

[80] M. Mikami and K. Ozaki, J. Phys.: Conf. Ser. **379**, 012006 (2012).

[81] S. Harada, K. Tanaka, and H. Inui, J. Appl. Phys. **108**, 083703 (2010).

[82] S. Bhattacharya, N. S. H. Gunda, R. Stern, S. Jacobs, R. Chmielowski, G. Dennler, and G. K. H. Madsen, Phys. Chem. Chem. Phys. **17**, 9161 (2015).

[83] We plot the direction of S and σ, which results in the maximum power factor.

[84] L. D. Hicks and M. S. Dresselhaus, Phys. Rev. B **47**, 12727 (1993).

[85] G. Hautier, A. Miglio, D. Waroquiers, G.-M. Rignanese, and X. Gonze, Chem. Mater. **26**, 5447 (2014).